Evaluating small coronary stents with dual-source photon-counting computed tomography: effect of different scan modes on image quality and performance in a phantom

Thomas Stein[1]
Constantin von zur Muhlen[2]
Niklas Verloh[1]
Till Schürmann[1]
Tobias Krauss[1]
Martin Soschynski[1]
Dirk Westermann[2]
Jana Taron[1]
Elif Can[1]
Christopher L. Schlett[1]
Fabian Bamberg[1]
Christopher Schuppert[1]
Muhammad Taha Hagar[1]

[1]Medical Center-University of Freiburg Faculty of Medicine, Department of Diagnostic and Interventional Radiology, Freiburg, Germany

[2]Medical Center-University of Freiburg Faculty of Medicine, Department of Cardiology and Angiology, Freiburg, Germany

Corresponding author: Muhammad Taha Hagar

E-mail: taha.hagar@uniklinik-freiburg.de

PURPOSE

The study aimed to assess the feasibility and image quality of dual-source photon-counting detector computed tomography (PCD-CT) in evaluating small-sized coronary artery stents with respect to different acquisition modes in a phantom model.

METHODS

Utilizing a phantom setup mimicking the average patient's water-equivalent diameter, we examined six distinct coronary stents inflated in a silicon tube, with stent sizes ranging from 2.0 to 3.5 mm, applying four different CT acquisition modes of a dual-source PCD-CT scanner: "high-pitch," "sequential," "spiral" (each with collimation of 144 × 0.4 mm and full spectral information), and "ultra-high-resolution (UHR)" (collimation of 120 × 0.2 mm and no spectral information). Image quality and diagnostic confidence were assessed using subjective measures, including a 4-point visual grading scale (4 = excellent; 1 = non-diagnostic) utilized by two independent radiologists, and objective measures, including the full width at half maximum (FWHM).

RESULTS

A total of 24 scans were acquired, and all were included in the analysis. Among all CT acquisition modes, the highest image quality was obtained for the UHR mode [median score: 4 (interquartile range (IQR): 3.67–4.00)] (P = 0.0015, with 37.5% rated as "excellent"), followed by the sequential mode [median score: 3.5 (IQR: 2.84–4.00)], P = 0.0326 and the spiral mode [median score: 3.0 (IQR: 2.53–3.47), P > 0.05]. The lowest image quality was observed for the high-pitch mode [median score: 2 (IQR: 1– 3), P = 0.028]. Similarly, diagnostic confidence for evaluating stent patency was highest for UHR and lowest for high-pitch (P < 0.001, respectively). Measurement of stent dimensions was accurate for all acquisition modes, with the UHR mode showing highest robustness (FWHM for sequential: 0.926 ± 0.061 vs. high-pitch: 0.990 ± 0.083 vs. spiral: 0.962 ± 0.085 vs. UHR: 0.941 ± 0.036, P = non-significant, respectively).

CONCLUSION

Assessing small-sized coronary stents using PCD-CT technology is feasible. The UHR mode offers superior image quality and diagnostic confidence, while all modes show consistent and accurate measurements.

CLINICAL SIGNIFICANCE

These findings highlight the potential of PCD-CT technology, particularly the UHR mode, to enhance non-invasive coronary stent evaluation. Confirmatory research is necessary to influence the guidelines, which recommend cardiac CT only for stents of 3 mm or larger.

KEYWORDS

Computed tomography, coronary artery, stents, technology

Coronary computed tomography (CT) computed tomography angiography (CTA) is an indispensable diagnostic tool for ruling out obstructive coronary artery disease (CAD) in patients with a low to intermediate risk profile.[1] While its use in patients with pre-existing CAD is generally more restrained, recent guidelines have acknowledged its reasonable use in assessing stent patency for patients experiencing symptomatic changes and if stents with an internal diameter of 3 mm or greater are present.[2,3] This is attributed to the diagnostic difficulties introduced by blooming artifacts, which originate from stent materials and consequently restrict the effectiveness of CTA-hence the restraint regarding larger stent diameters.[4,5]

With the clinical introduction of novel photon-counting detector (PCD) CT technology, there is a potential advancement in overcoming these challenges. This technology eliminates the need for septa within the detector elements and allows improvement in geometrical dose efficiency and electrocardiogram (ECG)-synchronized CTA at ultra-high resolution (UHR) by utilizing a direct conversion process for incoming X-ray photons and semiconductor plate technology.[6] ECG-synchronized CTA is a special imaging procedure that is primarily used to examine the structure and function of the heart. In this method, the CT scanner is synchronized with the patient's ECG signal, allowing the scanner to acquire images at specific points in the cardiac function. This synchronization helps to reduce the motion artifacts caused by the beating heart, resulting in better and more detailed images of the heart and its vessels, which is crucial for the accurate diagnosis of heart diseases and conditions. More-

over, a dual-source CT system using PCD-CT technology is clinically available. Recent studies have demonstrated the potential of PCD-CT to reduce artifacts significantly and improve image quality in non-invasive stent assessment, compared with traditional energy-integrating detector (EID) CT.[7] Photon-CT utilizes detectors that do not require septa for lightning photons, unlike EID-CT. The PCD design incorporates application-specific integrated circuits instead of photodiodes, facilitating the construction of smaller detector pixels. As a result, PCD-CT achieves higher spatial resolution, better delineation of structure edges, and reduces the spread of signals from high-density objects, effectively mitigating blooming artifacts. Additionally, PCD-CT's capability to directly count and measure the energy of individual photons allows for precise material differentiation, minimizing the impact of overlapping densities. Moreover, PCD-CT reduces image noise by directly converting X-ray photons into electrical signals, enhancing image clarity and reducing blooming artifacts. Initial human and phantom studies have shown promising results for PCD-CT in stent evaluation, particularly when employing a sharp vascular convolution kernel.[8,9] This approach has facilitated excellent *in vivo* visualization of stent lumens, with a recent study achieving a 100% negative predictive value for stent patency evaluation against invasive angiography as the reference standard.[10]

However, a dedicated analysis of PCD-CT's performance in evaluating coronary artery stents with an internal diameter of 3 mm or less is lacking. Therefore, our study aims to evaluate the feasibility and assess the image quality of PCD-CT in evaluating small-sized coronary artery stents. Furthermore, we seek to investigate which specific scan mode provides the highest performance and image quality.

Methods

Ethical statement

This study used an *ex vivo* phantom model; therefore, ethical approval and the Dec-

laration of Helsinki were not applicable. The additionally presented *in vivo* case is part of a larger study sanctioned by the Institutional Review Board of University Medical Center, Freiburg (approval no: 21-2469, date: 09/21/2021), investigating the functionalities and properties of photon-counting CT in various clinical scenarios. Patient consent was not required.

Phantom setup

The experimental setup utilized in this current study was previously published.[11] A phantom mimicking the average (avg) patient's water-equivalent diameter (D_w) value was constructed based on the analysis of 457 consecutive patients (189 women, 268 men; age 61.15 ± 12.95 years; median body mass index 27.2; range 17.2–58.8) undergoing cardiac CT. The D_w value was calculated using a dose management system (DoseM, Infinitt EU, Frankfurt, Germany) according to AAPM TG220,[12] with an avg D_w of 27.5 cm determined. The phantom, comprising a polymethyl-methacrylate frame (36.0 × 24.5 cm) filled with tap water, achieved a D_w of 28.0 cm. For CT measurements, various stents were inflated within silicone tubes at pressures specified by the manufacturer's *in vitro* compliance table and mounted at the phantom's isocenter. Silicone tubes were chosen for their minimal interference in image quality.

Coronary stents

Six distinct coronary stents with small diameters were examined, each differing in size and from various manufacturers. The sizes of these stents ranged from 2.0 to 3.5 mm. The characteristics of each stent are shown in Table 1.

Contrast media

The stent-containing silicon tubes were filled with an iodinated contrast medium (Imeron 400, Bracco Imaging, Italy) and diluted to achieve a radiodensity of 800 Hounsfield units (HU) at a tube voltage of

Main points

- Evaluating small coronary stents with conventional computed tomography (CT) is challenging due to blooming artifacts.

- This study assessed dual-source photon-counting detector (PCD) CT using different acquisition modes in a phantom model.

- The ultra-high-resolution (UHR) mode provided the best image quality, with an excellent median score of 4.0, and the highest diagnostic confidence ($P < 0.001$).

- All scan modes showed consistent and accurate stent measurements, with the UHR mode scoring a full width at half maximum of 0.941 ± 0.036 mm.

- The use of PCD-CT technology is promising for non-invasive small-sized stent evaluation; further clinical validation is needed to initiate guideline revision.

Table 1. Characteristics of coronary stents used in the study, including size, length, and properties

Manufacturer	Name	Size (mm)	Length (mm)	Properties
Monorail	Synergy	3.50	8.00	Everolimus-eluting
Synsiro	Biotronik	3.00	26.00	Sirolimus-eluting
Monrail	Promus Elite	2.75	8.00	Everolimus-eluting
Monrail	Promus Elite	2.50	8.00	Everolimus-eluting
Monrail	Promus Elite	2.25	32.00	Everolimus-eluting
Medtronic	Resolute Onyx	2.00	12.00	Zotarolimus-eluting

120 kVp. To ensure an even distribution of the contrast agent and to prevent any sedimentation, a flow-simulating pump was incorporated into the phantom setup. This device was used to simulate a blood flow rate of 2.0 mL/s, mirroring physiological conditions. Details of the contrast medium specifications are presented in Table 2.

Computed tomography scan parameters and image reconstruction

All scans were performed on a 1st generation, dual-source PCD CT scanner (NAEOTOM Alpha, Siemens Healthineers AG, software version VA50). In total, four different scans were performed for each stent: 1) a prospectively ECG-synchronized high-pitch spiral CT ("flash"), 2) a prospectively ECG-triggered sequential scan ("sequential"), 3) a retrospectively ECG-gated spiral CT ("spiral"); all featured full spectral sensitivity and a collimation of 144 × 0.4 mm. Last, a retrospective spiral CT employing the ultrahigh-spatial-resolution scan mode ("UHR") without

Table 2. Contrast medium specifications

Iodine concentration (mgI/mL)	400
Volume (mL)	70
Flow rate (mL/s)	2.0
Iodine flux (g/s)	0.8
Total iodine dose (g)	28

spectral information and a collimation of 120 × 0.2 mm was acquired. The tube voltage was set at 120 kVp, and a constant effective tube current of 32 mAs was maintained across all scans to standardize image quality and ensure consistent diagnostic accuracy, in line with the manufacturer's recommendations for the CT scanner used. To mimic a typical z-axis extension of cardiac CT, the scan length was set at 120 mm each.[13,14] Images were reconstructed to a field of view of 140 × 140 mm and a matrix size of 512 × 512 pixels. Axial images were reconstructed employing an intermediate sharp vascular convolution kernel (Bv60) and Quantum Iterative Reconstruction at level 3. Detailed CT scan and reconstruction parameters are outlined in Table 3.

Computed tomography data analysis

All CT scans were evaluated by two independent board-certified radiologists (MTH, CS; 5 and 6 years of experience in cardiac CT, respectively) on a dedicated and clinically approved workstation (Dedalus HealthCare, Bonn, Germany). Images were provided in the transversal orientation, with a default window level of 850 HU and a window width of 2.200 HU. The readers were permitted to adjust the window settings as desired and to perform multiplanar reconstructions for their analysis.

Visual and subjective image quality assessment

The overall subjective image quality of the stented lumen was evaluated using a four-point visual grading scale, considering sharpness, noise, blooming artifact interference, and diagnostic confidence for assessing stent patency. The grading scale for each parameter was defined as follows: For overall image quality, a score of 1 indicated non-diagnostic quality, characterized by poor lumen attenuation with significant artifact interference from stent struts; a score of 2 indicated fair quality, with moderate interference from stent struts but interpretable lumen attenuation; a score of 3 represented good quality, with mild interference from stent struts and generally clear lumen attenuation; and a score of 4 indicated excellent quality, marked by clear lumen attenuation without artifact interference from stent struts.

Noise levels and blooming were scored inversely, with minimal noise or blooming receiving a score of 1 and extensive noise or blooming receiving a score of 4. Specifically, for noise levels, a score of 1 indicated minimal noise with a homogenous lumen appearance; a score of 2 indicated mild noise that did not significantly affect image interpretation; a score of 3 indicated moderate noise that may impact image clarity; and a score of

Table 3. Computed tomography scan and reconstruction parameters

	Flash	Sequential	Spiral	UHR
ECG-synchronization	Prospective	Prospective	Retrospective	Retrospective
Scan length (mm)	120	120	120	120
Scan direction	Cranio-caudal	Cranio-caudal	Cranio-caudal	Cranio-caudal
Tube voltage (kV)	120	120	120	120
Effective mAs	32	32	32	32
CARE IQ level	135	135	135	82
CTDI$_{vol}$ (mGy)	2.33	11.8	28.2	35.0
DLP (mGy x cm)	40.7	146	428	485
Rotation time (ms)	250	250	250	250
Pitch	3.2	N/A	0.2	0.2
Slice collimation (mm)	144 × 0.4	144 × 0.4	144 × 0.4	120 × 0.2
Slice width (mm)	0.4	0.4	0.4	0.2
Increment (mm)	0.2	0.2	0.2	0.1
Matrix size (pixels)	512 × 512	512 × 512	512 × 512	512 × 512
Field of view (mm)	140 × 140	140 × 140	140 × 140	140 × 140
Reconstruction kernel	Bv60	Bv60	Bv60	Bv60
Iterative reconstruction	QIR level 3	QIR level 3	QIR level 3	QIR level 3
Spectral reconstruction	Monoenergetic + 67 keV	Monoenergetic + 67 keV	Monoenergetic + 67 keV	Polychromatic (T3D)

ECG, electrocardiogram; CTDI$_{vol}$, computed tomography dose index volume; DLP, dose-length-product; N/A, not-applicable; QIR, quantum iterative reconstruction; UHR, ultra-high-resolution.

4 indicated extensive noise that made image interpretation difficult. For blooming artifact interference, a score of 1 indicated minimal blooming with clear visualization of stent struts; a score of 2 indicated mild blooming that did not significantly obscure stent struts; a score of 3 indicated moderate blooming that partially obscured stent struts; and a score of 4 indicated extensive blooming that significantly obscured stent struts.

Diagnostic confidence for evaluating in-stent lumen patency ranged from non-diagnostic (score of 1), where lumen patency could not be assessed, to reduced confidence (score of 2), where lumen patency assessment was possible but with reduced confidence, to good confidence (score of 3), where lumen patency could be assessed with good confidence, and ultimately to excellent confidence (score of 4), where lumen patency could be assessed with high confidence.

Quantitative objective image quality assessment

Full width at half maximum

Two readers measured coronary stent length and internal and external diameters on reformatted CT images, focusing on the axial slice that best-represented stent geometry. To quantify blooming systematically, sagittal cross-sectional images along the phantom's axis were first reconstructed. Subsequently, attenuation profiles were avg over multiple voxels perpendicular to the longitudinal axis of the stent, establishing an avg attenuation profile. Utilizing these attenuation profiles, the full width at half maximum (FWHM) for both intensity peaks was calculated for all stents under each acquisition mode. The mean of these two FWHM values was then used to derive measurement consistency for the stent corresponding to each acquisition mode, as depicted in Figure 1.

Effect on in-stent lumen attenuation, contrast-to-noise ratio, and signal-to-noise ratio

Three manually drawn regions of interest (ROIs) were performed: an in-stent ROI (ROI_{in_stent}), carefully avoiding stent struts with a minimum 4 mm^2 area, and two identical-sized ROIs at the adjacent vessel lumen relative to the stent ($ROI_{proximal\ vessel}$ and $ROI_{distal\ vessel}$), placed within 10 mm of the stent's ends. The avg HU and standard deviation (SD) were noted for every ROI. The following equation was applied to evaluate the attenuation changes caused by the stent in the lumen ($HU_{In-stent}$):

$$HU_{In\_stent} = avgHU_{in\_stent} - \frac{avgHU_{proximal\ vessel} + avgHU_{distal\ vessel}}{2}$$

Two circular ROIs of 250 mm^2 were placed within the water around the stent, and the avg, as well as SD and HU, were noted. The signal-to-noise ratio (SNR) and contrast-to-noise ratio (CNR) were calculated as follows:

$$SNR = \frac{avgHU\ vessel}{SD\ HU\ water} \qquad CNR = \frac{avgHU\ vessel - avg\ HU\ water}{SD\ HU\ water}$$

Statistical analyses were performed using open-source Python (version 3.9.13) and Jupyter Notebooks. The Shapiro–Wilk test was used to check for the presumption of normal distribution. Quantitative variables with normal distribution were expressed as mean ± SD. Categorical variables were presented as frequencies and percentages in parentheses. Non-normally distributed variables, such as subjective image quality scores or attenuation, were expressed as the median and interquartile range (IQR), and their comparisons across different acquisition modes were analyzed using the Kruskal–Wallis test. Analysis of variance (ANOVA) was performed to determine the statistical significance of the differences in FWHM measurements across the four CT acquisition modes. Following a significant ANOVA result, post-hoc pairwise comparisons were conducted using Tukey's honestly significant difference (HSD) test to identify which specific acquisition modes differed from one another. To account for the increased risk of type I error due to multiple comparisons, the Bonferroni correction was applied to all P values. A P value of <0.05 was considered statistically significant. For testing diagnostic accuracy, 95% confidence intervals (CIs) were reported. All statistical measurements were performed by TS (4 years of experience).

Results

For all six small-sized stents, four consecutive scans using different acquisition methods were performed. Representative images for a stent measuring 2.0 mm in diameter are presented in Figure 2. Figure 3 summarizes the overall subjective assessments of diagnostic confidence for evaluating stent patency, sharpness, blooming artifact interference, and noise; Table 3 outlines the overall image quality and objective quality evaluation metrics.

Visual and subjective image quality assessment

The UHR mode provided the highest subjective image quality across all stent sizes, with a median score of 4 (CI: 3.67–4.00), categorizing 18 (37.5%) of the images as "excellent." Sequential and spiral modes showed slightly lower subjective image quality, with median values of 3.5 (CI: 2.84–4.00) and 3.0 (CI: 2.53–3.47), respectively. The flash mode provided the lowest subjective image quality, with a median value of 2.25 (CI: 1.66–2.84)) and was considered "non-diagnostic"
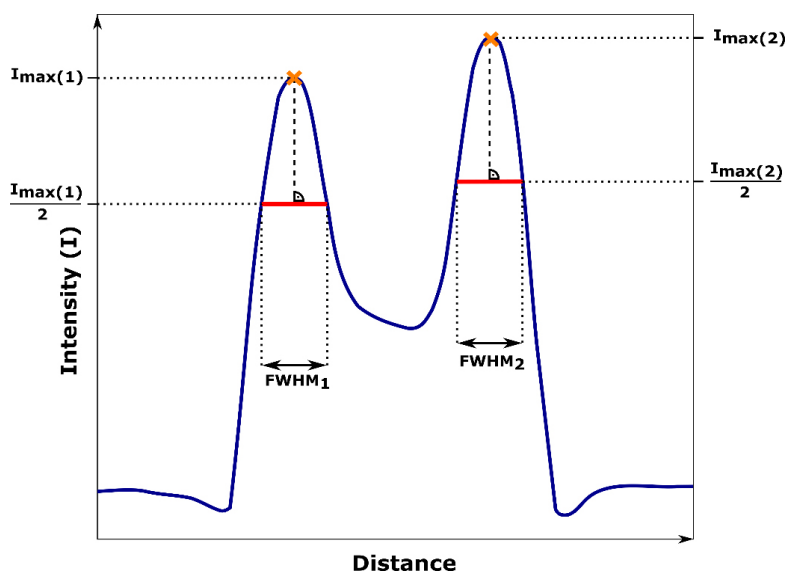

Figure 1. Displays the mean intensity profile of an entire stent. For every acquisition mode and each stent, the full width at half diameter was calculated to account objectively for stent-induced blooming artifact interference. FWHM, full width at half maximum.

in 3 (6.3%) stents. Subjective and objective image qualities relative to the acquisition mode are displayed in Table 4.

When analyzing the acquisition modes in detail for different stent sizes, the UHR mode provided the highest performance in terms of image quality across various stent diameters, with statistically significant differences identified when compared with the flash mode (CI: 1.31–2.85, $P = 0.0015$) and when compared with the spiral mode (CI: 2.38-3.69, $P = 0.0284$). The sequential mode did not differ significantly from the UHR-spiral mode in pairwise comparisons (CI: 2.47–4.11, $P = 0.3236$). Details on subjective image quality distribution relative to stent size are provided in Table 5.

Visual and subjective sharpness analysis

The analysis of stent sharpness revealed that the UHR mode was significantly associated with the highest mean sharpness scores across all stent sizes, achieving a value of 4.00 (CI: 3.67–4.33), whereas the flash mode achieved a median value of 2.00 (CI: 1.97–2.21). The sequential mode showed moderate performance, with a score of 3.00 (CI: 2.53–3.47), whereas the spiral mode showed a median of 2.50 (CI: 1.8–3.20), with $P = 0.0349$ compared with the UHR mode. Stent sizes did not affect overall sharpness (Tukey HSD $P > 0.05$). Overall, the statistical analysis emphasizes the superior performance of the UHR mode regarding sharpness across the range of stent diameters. Significant differences were found in comparisons with the flash mode ($P = 0.0007$) and spiral mode ($P = 0.0349$), and again, the sequential mode's differences were not significant ($P = 0.2279$).

Visual and subjective noise analysis

The analysis of noise levels across different stent sizes and acquisition modes revealed that the UHR-spiral mode was associated with the highest mean noise level of 3.00 (CI: 2.67–3.33), indicating it produced the most noise among the acquisition modes tested. In contrast, the flash mode showed improved noise performance with 2.25 (CI: 1.34–2.66), with significant differences compared with UHR ($P = 0.0217$). Sequential and spiral modes demonstrated intermediate noise levels with 2.50 (CI: 1.84–3.16) and 2.25 (CI: 1.70–2.80), respectively. Analysis of noise levels in relation to stent diameters did not show significant variation (Tukey HSD $P > 0.05$, respectively).

Visual and subjective diagnostic confidence for evaluating stent patency

In evaluating coronary stents using the different cardiac CT scan modes-sequential, spiral, UHR, and flash-the results showed a median "good" diagnostic confidence of 3.0 (IQR, 2.0–4.0) for sequential, for spiral a "good" median score of 3.0 (IQR, 3.0–4.0), and for flash a "reduced" median score of 2.0 (IQR, 2.0–3.0). The UHR mode provided the highest diagnostic confidence median of 3.5, with an IQR of 1.0 (3.0–4.0). The UHR mode demonstrated superior performance by achieving "good" or "excellent" diagnostic confidence in all readings (n = 12), which corresponds to 100.00% of its evaluations. The spiral scan mode followed, achieving "good" or "excellent" diagnostic confidence in 9 out of 12 readings (75%). The sequential scan mode reported "good" or "excellent" confidence levels in 9 out of 12 readings, translating to 75% of the time, while the flash scan mode achieved these levels of confidence in 3 instances or 25% of cases. Detailed metrics on diagnostic confidence are presented in Table 6, and an *in vivo* imaging example is provided in Figure 4.

Full width at half maximum measurements

The inner stent diameters were consistently measured across all modes, averaging 1.8 ± 0.4 mm; the outer diameter measurements showed a slight variation, with an overall avg of 3.1 ± 0.5 mm. The FWHM values were uniformly distributed, with a mean of 0.947 ± 0.067 mm across all scans.

The most stable mean FWHM was found to be 0.941 mm (CI: 0.912–0.971) in the UHR mode, followed by the sequential mode (FWHM of 0.926, CI: 0.876–0.975), indicating the least amount of blooming artifact interference. The flash mode displayed the highest mean FWHM of 0.990 mm (CI: 0.924–1.057), potentially indicating more blooming susceptibility. However, the differences across acquisition modes did not reach statistical significance (ANOVA $P = 0.386$). The sequential and spiral modes yielded similar mean FWHM results of 0.926 mm (CI: 0.877–0.975) and 0.932 mm (CI: 0.863–1.000), respectively, with no significant differences compared with the UHR-spiral mode (Bonferroni corrected $P > 0.05$).
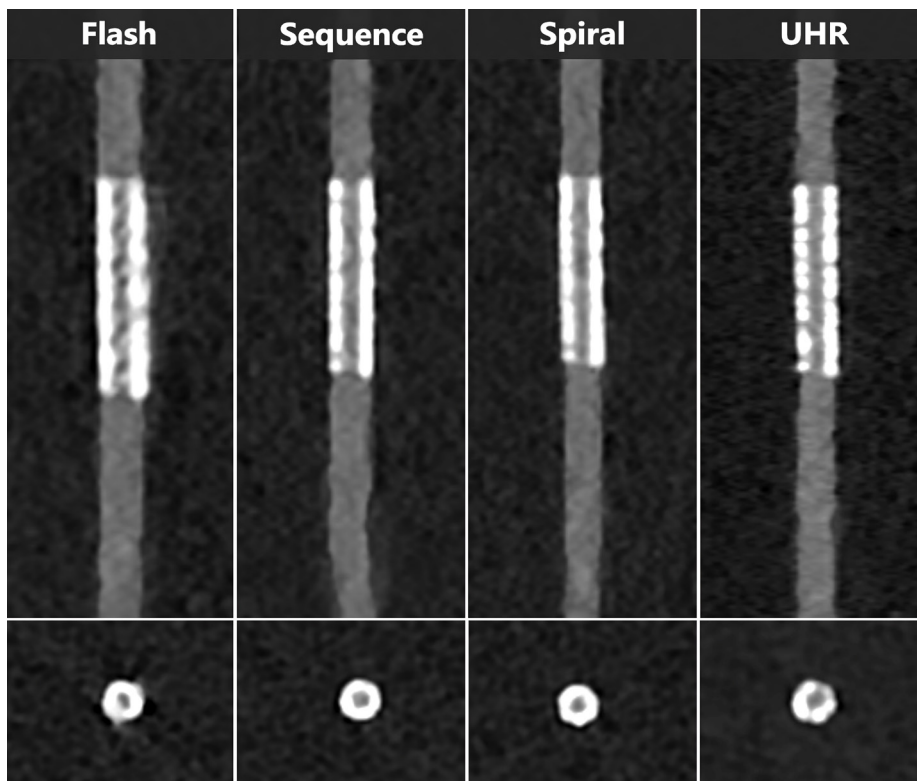

Figure 2. Presents a longitudinal multiparametric reconstruction alongside a transversal section through a stent of 2.00 mm, with a window level of 850 Hounsfield units (HU) and a window width of 2,200 HU. Displayed are, from left to right, four distinct computed tomography (CT) acquisition modes: high-pitch helical CT ("flash"), sequential CT, spiral CT, and ultra-high-resolution (UHR) CT. Image quality was assessed by two independent radiologists, who found the flash CT quality poor due to compromised clarity and artifact interference of the stented lumen. Both sequential and spiral CT images were deemed to have reduced quality, with some loss of detail within the stent lumen. In contrast, the UHR CT image was rated independently as excellent, showcasing exceptional detail and clarity in stent structure and lumen visualization.
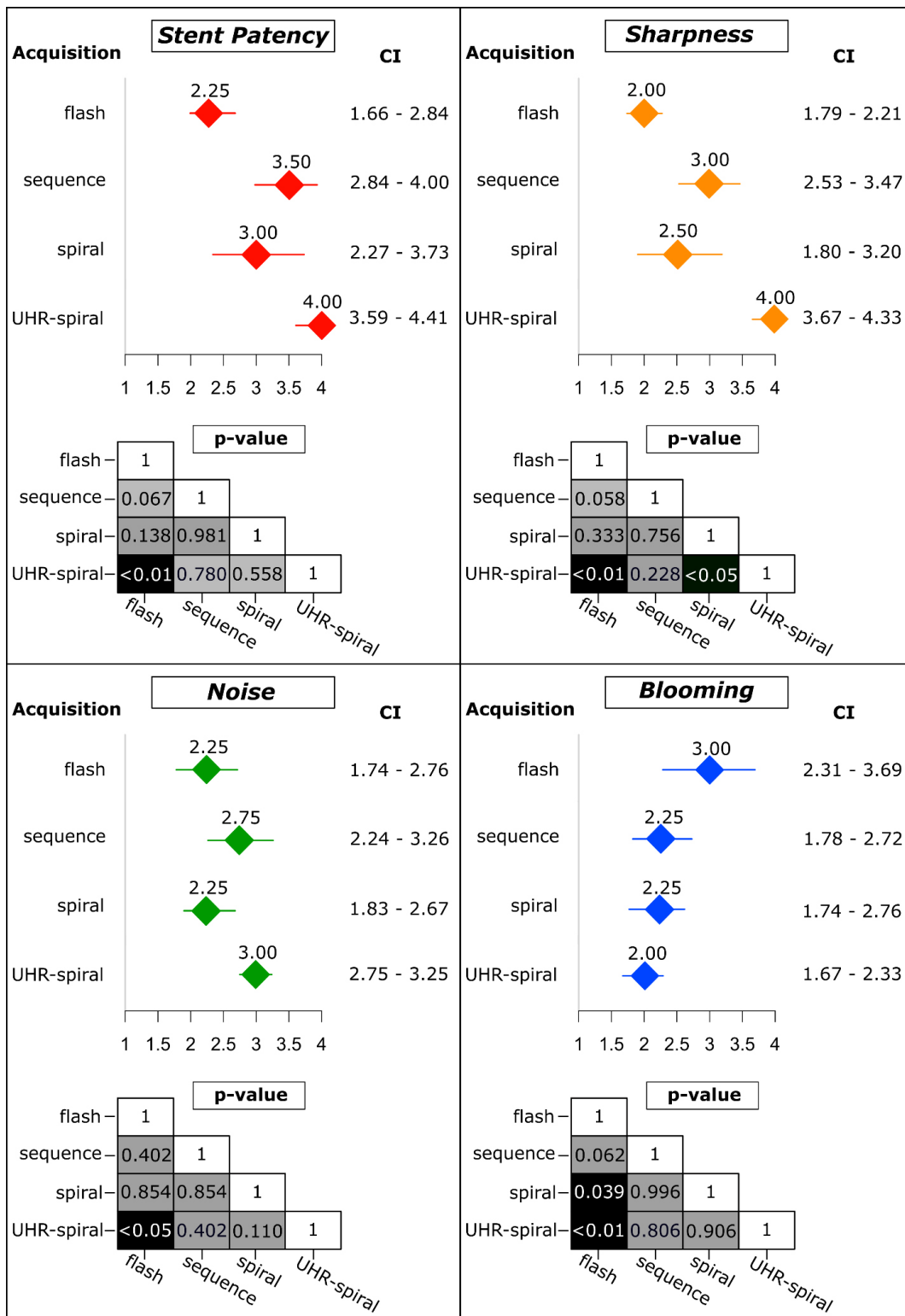
Figure 3. Displays the result of the qualitative analysis for diagnostic confidence of stent patency (upper left), sharpness (upper right), noise (lower left), and blooming artifact interference (lower right). Values were presented as mean and 95% confidence interval ranges (CI). The P values were corrected for multiple comparisons using the Bonferroni method. The ultra-high-resolution (UHR)-spiral mode received the highest ratings for stent patency with a mean of 4.00 (CI: 3.59–4.41), and flash mode showed the lowest with a mean of 2.25 (CI: 1.66–2.84). Similarly, sharpness was rated highest in the UHR-spiral mode with a mean of 4.00 (CI: 3.67–4.33). Flash mode registered the lowest sharpness ratings with a mean of 2.00 (CI: 1.79–2.21). Regarding noise, the UHR-spiral mode exhibited the lowest perceived noise levels with a mean of 3.00 (CI: 2.75–3.25), while the sequential mode also displayed comparatively low noise levels with a mean of 2.75 (CI: 2.24–3.26). For blooming effects, the flash mode exhibited the highest with a mean of 3.00 (CI: 2.31–3.69), and the lowest blooming effects were noted in the UHR-spiral mode with a mean of 2.00 (CI: 1.67–2.33).

Table 4. Image quality analysis with analysis of overall image quality, diagnostic confidence, and objective measurements across different computed tomography acquisition modes: overall image quality (median [IQR]), diagnostic confidence (median [IQR]), inner diameter (mm, mean ± SD), outer diameter (mm, mean ± SD), FWHM (mm, mean ± SD), SNR (mean ± SD) and CNR (mean ± SD)

	Flash	Sequential	Spiral	UHR	Overall
Subjective image quality					
Overall image quality[†]	2 [1–3]	3 [2–4]	3 [2–4]	4 [3–4]	3 [2–4]
Excellent		3	6	9	18 (37.5%)
Good	4	7	3	3	17 (35.4%)
Reduced	5	2	3		10 (20.8%)
Non-diagnostic	3				3 (6.3%)
Objective image quality					
Measured inner diameter (mm)	1.79 ± 0.33	1.81 ± 0.31	1.77 ± 0.35	1.71 ± 0.27	1.8 ± 0.4
Measured outer diameter (mm)	3.02 ± 0.47	3.17 ± 0.38	3.15 ± 0.39	3.15 ± 0.35	3.1 ± 0.5
FWHM (mm)	0.990 ± 0.083	0.926 ± 0.061	0.962 ± 0.085	0.941 ± 0.036	0.947 ± 0.067
Attenuation (avg HU)					
Water*	5.23 ± 57.0	4.64 ± 52.5	6.26 ± 51.5	3.43 ± 43.6	4.89 ± 51.2
Adjacent vessel*	863.5 ± 56.1	857.4 ± 58.5	853.5 ± 59.0	750.7 ± 49.95	831.3 ± 55.9
In-stent lumen*	991.5 ± 140.1	923.1 ± 95.1	928.0 ± 82.5	817.4 ± 83.5	915.0 ± 100.3
Noise (SD HU)					
Water	50.1	49.4	53.4	51.8	51.2 ± 6.6
SNR	11.6 ± 1.8	13.6 ± 1.9	14.0 ± 2.1	13.4 ± 1.7	13.2 ± 2.1
CNR	11.6 ± 1.9	13.5 ± 1.9	13.9 ± 2.1	13.4 ± 1.7	13.1 ± 2.1

[†]Values correspond to median and interquartile range in square brackets; *Values are presented as mean and standard deviation.
FWHM, full width at half maximum; SNR, signal-to-noise ratio; CNR, contrast-to-noise ratio; avg, average; HU, Hounsfield units; SD, standard deviation; IQR, interquartile range; UHR, ultra-high-resolution.

Table 5. Image quality relative to acquisition mode and stent size

		2.00	2.25	2.50	2.75	3.00	3.50	Image quality
				Stent size (mm)				
Scan mode	Flash							Excellent (n = 18)
	Sequential					1	2	
	Spiral		1	1		2	2	
	UHR	2		2	1	2	2	
	Flash		1		2	1		Good (n = 17)
	Sequential	1	2	1	2	1		
	Spiral		1	1	1			
	UHR		2		1			
	Flash		1	2		1	1	Reduced (n = 10)
	Sequential	1		1				
	Spiral	2			1			
	UHR							
	Flash	2					1	Non-diagnostic (n = 3)
	Sequential							
	Spiral							
	UHR							

Two readers assessed the image quality for various stent sizes across different imaging acquisition protocols. The stents ranged in size from 2.00 to 3.50 mm, with protocols including flash, sequential, spiral, and UHR scan modes. Image quality was rated on a four-point scale from "excellent" to "non-diagnostic." Each entry represents the number of stents that were assigned a particular image quality level by the readers under each protocol and stent size combination. The far-right column denotes the total counts of ratings for each image quality category. UHR, ultra-high resolution.

Table 6. Diagnostic confidence relative to acquisition mode and stent size

Scan mode		Stent size (mm)						Diagnostic confidence
		2.00	2.25	2.50	2.75	3.00	3.50	
	Flash							Excellent (n = 19)
	Sequential		1		2	1	2	
	Spiral			1		2	2	
	UHR	2		2		2	2	
	Flash		1		2	1		Good (n = 15)
	Sequential		1	1		1		
	Spiral		2		2			
	UHR		2		2			
	Flash		1	2		1	1	Reduced (n = 10)
	Sequential	2		1				
	Spiral	1		1				
	UHR							
	Flash	2					1	Poor (n = 4)
	Sequential							
	Spiral	1						
	UHR							

Two readers assessed the diagnostic confidence for various stent sizes across different imaging acquisition protocols. The stents ranged in size from 2.0 to 3.50 mm, with protocols including flash, sequential, spiral, and UHR mode. Diagnostic confidence was rated on a four-point scale from "excellent" to "poor." Each entry represents the number of stents that were assigned a particular confidence level by the readers under each protocol and stent size combination. The far-right column denotes the total counts of ratings for each diagnostic confidence category. UHR, ultra-high resolution.

Signal-to-noise ratio and contrast-to-noise ratio

The SNR values spanned from 11.6 ± 1.8 in flash mode to 14.0 ± 2.1 in spiral mode. Similarly, CNR evaluations illustrated a marginal preference for the spiral mode at 13.9 ± 2.1 over the flash mode, which presented a CNR of 11.6 ± 1.9.

Discussion

Our *ex vivo* phantom study assessed the feasibility and image quality of PCD-CT for evaluating small-sized coronary stents (2.0–3.5 mm internal diameter). We found that PCD-CT is effective for stent imaging, particularly in the UHR mode, which provided superior image quality and diagnostic confidence compared with standard dual-source PCD-CT scan modes. The high-pitch spiral mode was deemed unsuitable for small stent imaging.

A study by Mannil et al.[15], which analyzed larger stents using a dual-source prototype scanner with one detector being an energy-integrating CT and the other using PCD technology, found that PCD technology enhanced stent lumen visibility. In comparative *in vitro* analysis between PCD-CT and EID-scanner systems, superior stent lumen visibility was achieved, particularly in the UHR mode.[16,17] The results of all these studies corroborate our findings.

The objective measures of the FWHM for the sequential and UHR modes underscored its superior robustness, while all acquisition modes provided measurement consistency. In that regard, our study results are in agreement with those of a recent study performed by Koons et al.[18], which shows the least amount of blooming for UHR mode and the use of a sharp kernel. This has been confirmed in a recent clinical study highlighting improved diagnostic performance of coronary stents with optimal in-stent lumen at Bv72 kernels.[19] Subjective assessments of image quality and diagnostic confidence further reinforced the advantages of the UHR mode, with it receiving the highest proportion of "excellent" ratings across all evaluated parameters. Conversely, the high-pitch helical scan mode displayed limitations in accurately depicting smaller stents, suggesting that although it may offer reduced radiation dose,[20] it is not suitable for small-sized stent assessment. This is confirmatory to results reported by Ochs et al.[21], where a noticeable deterioration in image quality was observed in patients with increased coronary calcifications.

While our results indicate a significant potential of UHR PCD-CT in assessing small-sized stents, the implications extend beyond stent evaluation: initial clinical studies indicate high potential in coronary stenosis of stenosis severity,[22] enhanced diagnostic accuracy in challenging cases, and pronounced plaques evaluation.[23-25] It remains to be determined how this advanced technology will impact patient management and outcomes.

This study's limitations include its *ex vivo* nature, which presents challenges for direct clinical application. We focused on different acquisition modes for small-sized stent image quality but did not evaluate the impact of different kernels or iterative reconstruction levels, which have been addressed in previous studies. Additionally, the current scanner software does not support simultaneous UHR–CTA spectral sensitivity with monoenergetic reconstruction, an area needing future research to determine the best imaging approach. In this regard, a recent study investigated the image quality of stents in various 3.00 mm stents UHR-CT with a sharp kernel, and synthetic monoenergetic reconstruction of 55 keV showed promising results.[26] Furthermore, updated scanner versions introduced sequential scanning with UHR. Here, a comparative analysis of diagnostic performance between retrospective

Figure 4. A practical instance of photon-counting detector computed tomography has demonstrated its successful use in a clinical setting for assessing coronary stents. The figure depicts a 48-year-old man with a clinical history of NSTEMI 2 years ago, necessitating emergent coronary stent implantations, as visualized by ultra-high-spatial resolution photon-counting coronary computed tomography angiography. **(a)** Cinematic rendering illustrates the presence of dual stents within the right coronary artery (RCA) and singular stents in the left anterior descending artery (LAD) and left circumflex coronary artery. **(b)** Transversal section depicts the stent at the posterolateral branch of the RCA with an internal diameter of 2.50 mm. **(c)** Curved multiplane reformation of each artery showcases the stent patency and provides superior visualization of the stent lumen for all stents, including the small-sized stent in the distal LAD (2.25 mm) and the posterolateral branch of the RCA (2.00 mm).

and sequential UHR PCD-CT would be insightful.

In conclusion, our *ex vivo* study demonstrates that the UHR mode of PCD-CT offers the best image quality and diagnostic confidence for evaluating small-sized coronary stents. Given that current guidelines do not recommend non-invasive modalities for stents smaller than 3 mm, our findings suggest that PCD-CT could fill this gap, pending validation through dedicated *in vivo* clinical studies.

Conflict of interest disclosure

Fabian Bamberg Siemens Healthineers AG (unrestricted research grant, speaker's bureau), Christopher L. Schlett Siemens Healthineers AG (speaker's bureau), Muhammad Taha Hagar Siemens Healthineers AG (speaker's bureau). Other authors have nothing to disclose.

References

1. Knuuti J. 2019 ESC Guidelines for the diagnosis and management of chronic coronary syndromes The Task Force for the diagnosis and management of chronic coronary syndromes of the European Society of Cardiology (ESC). *Russ J Cardiol*. 2020;25(2):3557. [CrossRef]

2. Gulati M, Levy PD, Mukherjee D, et al. 2021 AHA/ACC/ASE/CHEST/SAEM/SCCT/SCMR Guideline for the Evaluation and Diagnosis of Chest Pain: a report of the American College of Cardiology/American Heart Association Joint Committee on Clinical Practice Guidelines. *Circulation*. 2021;144(22):e368-e454. Erratum in: *Circulation*. 2023;148(24):e281. [CrossRef]

3. Narula J, Chandrashekhar Y, Ahmadi A, et al. SCCT 2021 expert consensus document on coronary computed tomographic angiography: a report of the society of cardiovascular computed tomography. *J Cardiovasc Comput Tomogr*. 2021;15(3):192-217. [CrossRef]

4. Pack JD, Xu M, Wang G, Baskaran L, Min J, De Man B. Cardiac CT blooming artifacts: clinical significance, root causes and potential solutions. *Vis Comput Ind Biomed Art*. 2022;5(1):29. [CrossRef]

5. Gilard M, Cornily JC, Pennec PY, et al. Assessment of coronary artery stents by 16 slice computed tomography. *Heart*. 2006;92(1):58-61. [CrossRef]

6. Mergen V, Sartoretti T, Baer-Beck M, et al. Ultra-High-Resolution Coronary CT angiography with photon-counting detector CT: feasibility and image characterization. *Invest Radiol*. 2022;57(12):780-788. [CrossRef]

7. Boccalini S, Si-Mohamed SA, Lacombe H, et al. First in-human results of computed tomography angiography for coronary stent assessment with a spectral photon counting computed tomography. *Invest Radiol*. 2022;57(4):212-221. [CrossRef]

8. Geering L, Sartoretti T, Mergen V, et al. First in-vivo coronary stent imaging with clinical ultra high resolution photon-counting CT. *J Cardiovasc Comput Tomogr*. 2023;17(3):233-235. [CrossRef]

9. Decker JA, O'Doherty J, Schoepf UJ, et al. Stent imaging on a clinical dual-source photon-counting detector CT system-impact of luminal attenuation and sharp kernels on lumen visibility. *Eur Radiol*. 2023;33(4):2469-2477. [CrossRef]

10. Hagar MT, Soschynski M, Saffar R, et al. Ultra-high-resolution photon-counting detector CT in evaluating coronary stent patency: a comparison to invasive coronary angiography. *Eur Radiol.* 2024;34(7):4273-4283. [CrossRef]

11. Stein T, Taron J, Verloh N, et al. Photon-counting computed tomography of coronary and peripheral artery stents: a phantom study. *Sci Rep.* 2023;13(1):14806. [CrossRef]

12. McCollough C, Bakalyar DM, Bostani M, et al. Use of water equivalent diameter for calculating patient size and size-specific dose estimates (SSDE) in CT: the report of AAPM Task Group 220. *AAPM Rep.* 2014;2014:6-23. [CrossRef]

13. Leschka S, Kim CH, Baumueller S, et al. Scan Length Adjustment of CT coronary angiography using the calcium scoring scan: effect on radiation dose. *AJR Am J Roentgenol.* 2010;194(3):272-277. [CrossRef]

14. Hagar MT, Soschynski M, Benndorf M, et al. Enhancing radiation dose efficiency in prospective ECG-triggered coronary CT angiography using calcium-scoring CT. *Diagnostics (Basel).* 2023;13(12):2062. [CrossRef]

15. Mannil M, Hickethier T, von Spiczak J, et al. Photon-counting CT: high-resolution imaging of coronary stents. *Invest Radiol.* 2018;53(3):143-149. [CrossRef]

16. Symons R, De Bruecker Y, Roosen J, et al. Quarter-millimeter spectral coronary stent imaging with photon-counting CT: Initial experience. *J Cardiovasc Comput Tomogr.* 2018;12(6):509-515. [CrossRef]

17. Petritsch B, Petri N, Weng AM, et al. Photon-counting computed tomography for coronary stent imaging: in vitro evaluation of 28 coronary stents. *Invest Radiol.* 2021;56(10):653-660. [CrossRef]

18. Koons EK, Thorne JE, Huber NR, et al. Quantifying lumen diameter in coronary artery stents with high-resolution photon counting detector CT and convolutional neural network denoising. *Med Phys.* 2023;50(7):4173-4181. [CrossRef]

19. Qin L, Zhou S, Dong H, et al. Improvement of coronary stent visualization using ultra-high-resolution photon-counting detector CT. *Eur Radiol.* 2024. [CrossRef]

20. Rajiah PS, Dunning CAS, Rajendran K, et al. High-Pitch Multienergy Coronary CT angiography in dual-source photon-counting detector CT scanner at low iodinated contrast dose. *Invest Radiol.* 2023;58(9):681-690. [CrossRef]

21. Ochs MM, Andre F, Korosoglou G, et al. Strengths and limitations of coronary angiography with turbo high-pitch third-generation dual-source CT. *Clin Radiol.* 2017;72(9):739-744. [CrossRef]

22. Halfmann MC, Bockius S, Emrich T, et al. Ultrahigh-spatial-resolution photon-counting detector CT angiography of coronary artery disease for stenosis assessment. *Radiology.* 2024;310(2):e231956. [CrossRef]

23. Mergen V, Eberhard M, Manka R, Euler A, Alkadhi H. First in-human quantitative plaque characterization with ultra-high resolution coronary photon-counting CT angiography. *Front Cardiovasc Med.* 2022;9:981012. [CrossRef]

24. Hagar MT, Soschynski M, Saffar R, et al. Accuracy of ultrahigh-resolution photon-counting CT for detecting coronary artery disease in a high-risk population. *Radiology.* 2023;307(5):e223305. [CrossRef]

25. Eberhard M, Candreva A, Rajagopal R, et al. Coronary stenosis quantification with ultra-high-resolution photon-counting detector CT angiography. *JACC Cardiovasc Imaging.* 2024;17:342-344. [CrossRef]

26. Elias Michael A, Schoenbeck D, Michael Woeltjen M. Photon counting computed tomography of in-stent-stenosis in a phantom: Optimal virtual monoenergetic imaging in ultra high resolution. *Heliyon.* 2024;10(6):e27636. [CrossRef]